Earth Sciences
2026, Vol. 15, No. 6, pp. 265–274
https://doi.org/10.11648/j.earth.20261506.12

SciencePG
Science Publishing Group

Research Article

Three-Dimensional Alteration Zonation of the Duobuza Porphyry Copper Deposit from Drill-core and Surface Reflectance Spectroscopy

Zhengxuan Li, Fojun Yao*

Key Laboratory of Metallogeny and Resources Assessment, Institute of Mineral Resources, Chinese Academy of Geological Sciences, Beijing, China

Abstract

Reflectance spectroscopy can resolve alteration mineralogy at outcrop and drill-core scales, thereby complementing satellite observations that are restricted to exposed surfaces. This study integrated spectra from four drill holes and 15 surface samples at the Duobuza porphyry copper deposit in the Duolong ore district, Tibet, to characterize alteration in three dimensions. The drill core was measured at 0.8-1.5 m intervals, and the surface samples were distributed across lithological and alteration boundaries. Measurements covering 350-2,500 nm were obtained with an Analytical Spectral Devices FieldSpec Pro spectroradiometer and interpreted in PimaView 3.1. The identified assemblage comprises anhydrite, gypsum, muscovite, phengite, chlorite, epidote, calcite, halloysite, montmorillonite, and illite. Relative abundances of illite, chlorite, muscovite, and calcite were combined in an empirical alteration index that was applied consistently to drill-core and surface measurements. The index separates potassic-silicic, phyllic, and propylitic domains and supports a three-dimensional representation of their distribution. The resulting pattern broadly matches the available geological mapping. Lower index values in the potassic-silicic domain are spatially associated with higher copper (Cu) concentrations, whereas higher values in the propylitic domain coincide with lower Cu concentrations. This relationship provides a qualitative exploration guide rather than a calibrated grade predictor. Given the four-hole dataset and the irregular distribution of the 15 surface samples, the model is semiquantitative. Integrating surface and drill-core spectra extends alteration mapping below the exposed surface and provides a framework for future multi-source mineral-exploration studies.

Keywords

Alteration Index, Drill-core Spectroscopy, Duobuza Porphyry Copper Deposit, Hydrothermal Alteration, Short-wave Infrared, Three-Dimensional Modelling

1. Introduction

Fluid-rock interaction in porphyry copper systems produces alteration minerals whose spatial distribution can be used to interpret mineralized intrusions and guide exploration. Many hydrous and hydroxyl-bearing phases, including minerals containing Al-OH, Mg-OH, Fe-OH, or molecular water, dis-

*Correspondence: Fojun Yao (fjyao@sina.com)

Received: 17 October 2026; **Accepted:** 17 November 2026; **Published:** 25 November 2026

Copyright: © The Author(s), 2026. Published by Science Publishing Group. This is an **Open Access** article, distributed under the terms of the Creative Commons Attribution 4.0 License (http://creativecommons.org/licenses/by/4.0/), which permits unrestricted use, distribution and reproduction in any medium, provided the original work is properly cited.

play diagnostic absorptions across the visible and near-infrared (VNIR) and short-wave infrared (SWIR) regions [1-4]. These spectral responses allow field and laboratory measurements to complement geological mapping, petrography, and imaging-based remote sensing [5-10]. Similar mineralogical principles have been used to construct remote-sensing alteration models for porphyry copper deposits in China [11].

Surface alteration in the Duolong district has previously been investigated with Advanced Spaceborne Thermal Emission and Reflection Radiometer (ASTER), Landsat-8 Operational Land Imager (OLI), Gaofen-5, and WorldView-3 observations [12-18]. Those studies show that exposed phyllic, argillic, and propylitic assemblages can be differentiated spectrally. They do not, however, resolve whether the mapped assemblages continue beneath cover. Spectral measurements of drill core address this limitation by adding depth information in a mineralogical form that can be compared directly with surface observations.

Here, drill-core and surface reflectance spectra are combined to develop a three-dimensional alteration-zonation model for Duobuza. The study identifies the dominant spectrally responsive minerals, summarizes their relative abundances with an empirical index, maps alteration in both vertical and horizontal dimensions, and evaluates the resulting pattern against geological mapping and Cu distribution. Its principal extension beyond earlier surface-based work is the explicit use of drill-core spectra to connect exposed and subsurface alteration and to examine the spatial association between the index and Cu concentration.

2. Geological Setting

2.1. Location

The Duobuza porphyry copper deposit lies on the Duobuza highland northwest of Gaize County, Tibet, at approximately 83°25′-27′ E and 32°49′-51′ N. Elevations in the low- to moderate-relief mountain terrain average about 5,000 m and reach 5,040.9 m near the deposit. An unpaved road connects the site with Gaize County, roughly 90 km to the southeast [19, 25].

2.2. Regional and Deposit Geology

Regionally, Duobuza is situated in the western Bangongco-Nujiang metallogenic belt of the Tethyan-Himalayan domain. It lies close to the Bangongco-Nujiang suture, between the Qiangtang terrane to the north and the Gangdese-Nyainqentanglha terrane to the south [19, 25]. The exposed succession contains clastic sedimentary rocks, andesite, and sandy conglomerate affected to varying degrees by regional metamorphism. Volcanic, effusive, and shallow intrusive activity accompanied the development of east-west-, northeast-, and northwest-trending structures [21, 24, 25].

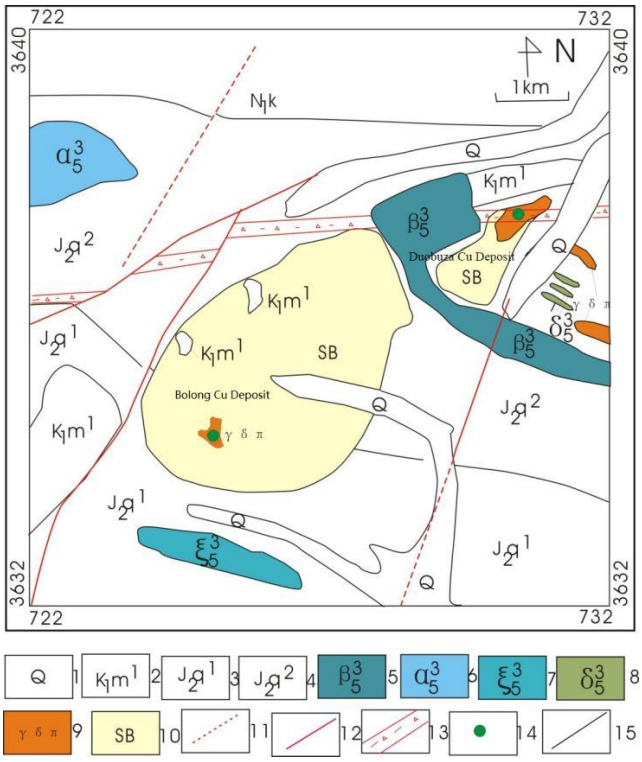

Figure 1. *Simplified geological map of the Duolong ore district.*

Map labels: Duobuza copper deposit and Bolong copper deposit. The numbered geological legend is translated in the following paragraph. Figure 1 legend: 1, Quaternary eluvial and colluvial deposits; 2, volcanic breccia in the upper member of the Lower Cretaceous Meiriqie Formation; 3, dark-gray silty slate with metamorphosed feldspathic quartz sandstone and limestone bands and lenses in Member 1 of the Middle Jurassic Quse Formation; 4, metamorphosed feldspathic quartz sandstone, siltstone and silty slate with siliceous rock, gray-green basalt and mafic lava in Member 2 of the Quse Formation; 5, epidotized basaltic andesite; 6, reddish-brown and brownish-gray andesite; 7, dacite; 8, gray-green diorite and quartz diorite; 9, granodiorite porphyry; 10, alteration zone; 11, inferred fault; 12, mapped fault of unknown type; 13, ductile-brittle fracture zone; 14, copper occurrence; 15, geological boundary.

Granodiorite porphyry and diorite porphyrite are the main intrusions within the Yanshiping Group and Meiriqie Formation; granodiorite, diabase porphyrite, diorite, and quartz diorite occur in smaller amounts. In the central-eastern part of the district, the mineralized granodiorite porphyry forms an irregular east-west-elongated body that intrudes its wall rocks. Geological studies record pervasive silicification, potassic alteration, chloritization, epidotization, and carbonatization and distinguish potassic, phyllic, argillic, and propylitic assemblages [25]. Fluid-inclusion evidence links the mineralization to hot, saline magmatic-hydrothermal fluids [20, 22, 23].

3. Materials and Methods

3.1. Spectral Instrumentation

Spectral acquisition followed established reflectance-measurement procedures [3, 10]. A FieldSpec Pro spectroradiometer manufactured by Analytical Spectral Devices recorded the 350-2,500 nm interval as 16-bit data, with 2 nm sampling in the SWIR region. For each sample, reflectance was obtained by normalizing the measured signal to that of a white reference panel with known reflectance.

3.2. Drill-core Sampling

The broader spectral campaign comprised four holes at Duobuza and four at Bolong [11]. Only the four Duobuza holes with matched coordinate, lithological, alteration, and Cu records were used in the present model. ZK2304 and ZK2312 occur on exploration line 23, whereas ZK701 and ZK708 occur on line 7; ZK701, ZK708, and ZK2304 intersect the intrusive body. ZK708 has a length of 447.49 m and was measured every 0.8 m. The corresponding lengths of ZK701, ZK2312, and ZK2304 are 288.56, 465.98, and 601.31 m, and spectra were collected at 1.5 m intervals in these three holes.

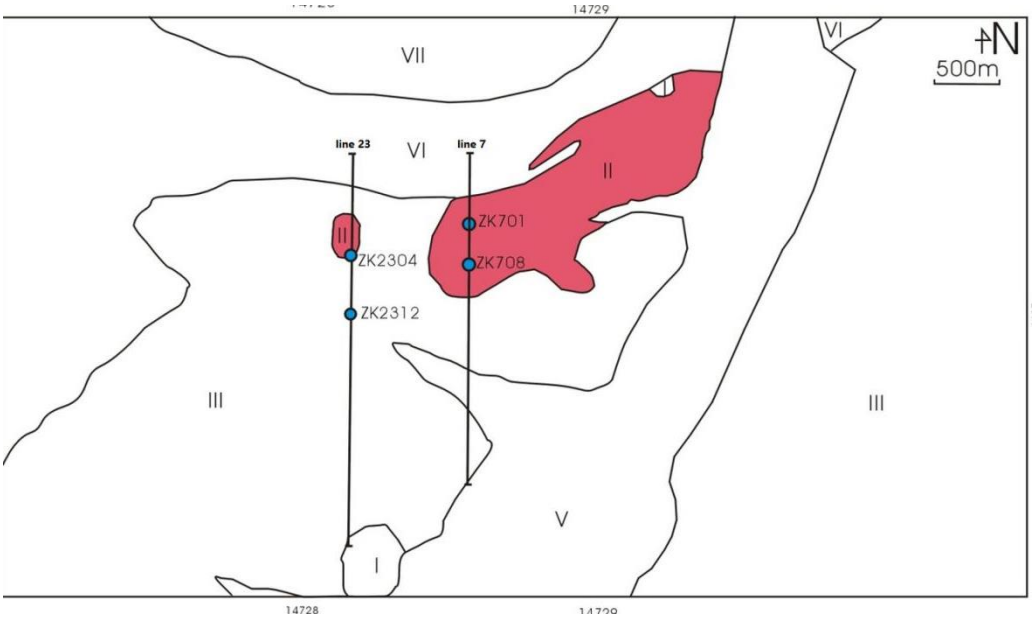

Figure 2. *Locations of spectrally measured drill holes at Duobuza.*

The labels 'line 23' and 'line 7' denote exploration lines 23 and 7, respectively.

Figure 2 legend: I, dark-green diabase; II, granodiorite porphyry and granodiorite; III, metamorphosed feldspathic quartz sandstone, siltstone, sandy slate, siliceous rock and gray-green basalt of the Middle Jurassic Quse Formation; V, Quaternary eluvial and colluvial deposits; VI, purplish-red volcaniclastic rocks with andesite porphyrite of the Lower Cretaceous Meiriqie Formation; VII, reddish-brown clay and sandy gravel of the Upper Tertiary Kangtuo Formation.

3.3. Surface Sampling

The horizontal analysis used 15 surface samples distributed irregularly across changes in lithology and alteration between the intrusive body and adjacent wall rocks (Figure 3). The sampled lithologies comprise metamorphosed quartz sandstone, granodiorite porphyry, lithic quartz sandstone, aplite, gabbro, breccia, granite, basaltic andesite, quartz porphyry, and schist. Field descriptions record limonitization, kaolinization, propylitic alteration, chloritization, and sericitization. Kaolinite was not used in the subsequent analysis because it occurred in too few samples. The sampling and spectral-processing framework derives from the broader Duolong campaign [11]; earlier surface-based alteration mapping of the district is reported by Yao et al. [15]. In the present study, the surface measurements provide the horizontal component for integration with drill-core spectra.

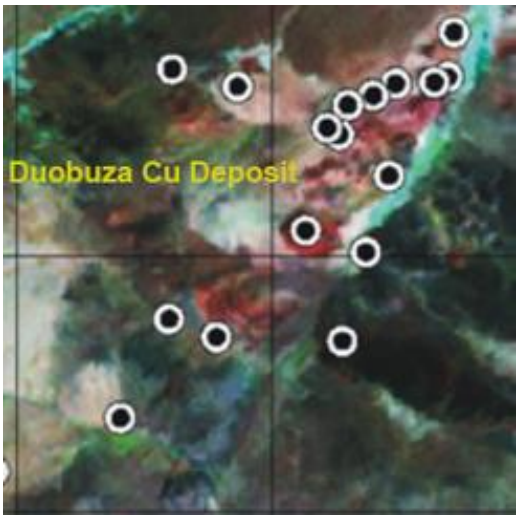

The yellow label identifies the Duobuza copper deposit.

Figure 3. *Locations of surface spectral samples at Duobuza.*

Table 1. *Surface samples used for horizontal alteration analysis.*

Sample	X	Y	Lithology	Field description
D36	728466.119	3633881.17	Gabbro	Gabbro-sandstone contact; dark-gray to gray-black gabbro and weakly metamorphosed quartz sandstone with chloritization and serpentinization.
D37	728650.453	3634575.837	Aplite	Dark-green massive aplite with a fine-grained texture and a 0.5 cm quartz vein.
D34	727106.257	3634053.273	Metamorphosed quartz sandstone	Gray metamorphosed quartz sandstone, locally containing lithic quartz sandstone.
D45	727131.684	3636004.849	Basaltic andesite	Black to dark-red basalt, identified by the No. 5 Geological Team as basaltic andesite; vesicular-amygdaloidal texture with amygdules filled by white plagioclase, K-feldspar and minor quartz.
D35	727479.083	3633910.817	Metamorphosed quartz sandstone	Yellow to pale-yellow quartz sandstone with aligned lithic fragments.
D44	727644.802	3635868.711	Quartz clastic rock	Flesh-red, very fine-grained quartz clastic rock with intense limonitization and a pink alunite-group mineral.
D38	728178.157	3634743.692	Gabbro	Gabbro with local epidotization of pyroxene.
D41	728346.994	3635545.87	Metamorphosed quartz sandstone	Yellow to grayish-yellow fine-grained quartz sandstone.
D40	728441.9	3635492.584	Metamorphosed quartz sandstone	Reddish-brown to yellowish-brown fine-grained quartz sandstone with jarosite alteration and limonitization.
D42	728509.379	3635725.307	Granodiorite porphyry	Malachite- and limonite-altered granodiorite porphyry; a shallow prospecting pit is present.
D43	728708.061	3635797.71	Granodiorite porphyry	Malachite- and azurite-altered granodiorite porphyry with feldspar, amphibole and minor quartz phenocrysts; a shallow prospecting pit is present.
D39	728831.836	3635171.81	Metamorphosed quartz sandstone	Reddish-brown to dark bluish-gray quartz sandstone; limonitized, massive and fine crystalline.

Sample	X	Y	Lithology	Field description
D09	728885.437	3635891.199	Quartz porphyry	Quartz porphyry exposed in a shallow prospecting pit, with strong limonitization, pyritization, azurite mineralization and intense alteration.
D08	729187.038	3635901.27	Granodiorite porphyry	Thick Quaternary cover; wash material comprises granodiorite porphyry with covellite and an oxidized coating; phenocrysts are quartz, feldspar and amphibole.
D07	729341.87	3636293.218	Metamorphosed quartz sandstone	Propylitized metamorphosed quartz sandstone with limonitization; massive, with a grayish-white fresh surface.

3.4. Mineral Identification and Alteration Index

Minerals were assigned in PimaView 3.1 by comparing each measured spectrum with a 36-entry reference library [7-9, 11]. The library includes water, actinolite, alunite, anhydrite, antigorite, apatite, aragonite, beryl, biotite, buddingtonite, calcite, Fe-rich chlorite, Mg-rich chlorite, Fe-Mg chlorite, diaspore, dickite, dolomite, epidote, gibbsite, gypsum, halloysite, hornblende, illite, jarosite, kaolinite, magnesite, montmorillonite, muscovite, nontronite, phengite, phlogopite, pyrophyllite, siderite, talc, tourmaline, and tremolite. Individual inspection generally yielded one to three mineral assignments and associated relative-abundance estimates per spectrum. Fe-rich, Mg-rich, and Fe-Mg chlorite were distinguished during interpretation and subsequently pooled as chlorite for zonation.

Illite, chlorite, muscovite and calcite were selected because they were consistently identified and collectively represented the observed zonation. The alteration index (AI) was calculated as follows:

$$AI = 0.160\ C_{illite} + 0.334\ C_{chlorite} + 0.334\ C_{muscovite} + 0.160\ C_{calcite} \quad (1)$$

In Equation (1), AI denotes the alteration index and C is the spectral estimate of relative mineral abundance. The empirical mineral-abundance framework follows the broader spectral study documented by Yao [11]. Sample and drill-core positions were used to join coordinate, lithological, alteration-mineral, and Cu records. Indexed drill-core measurements were then interpolated into vertical sections and three-dimensional surfaces, and Equation (1) was also evaluated for the surface samples. Class boundaries of 0.0664, 0.1336, and 0.2 separate the principal alteration domains. These empirically selected values reflect measured mineral distributions and drill logs; they do not quantify absolute alteration intensity.

4. Results

4.1. Spectrally Identified Alteration Assemblages

Interpretation of the Duobuza spectra yielded anhydrite, gypsum, muscovite, phengite, chlorite, epidote, calcite, halloysite, montmorillonite, and illite as the main alteration phases. Gypsum, halloysite, and montmorillonite are concentrated in the surface dataset and are therefore attributed mainly to supergene alteration or weathering. Phyllic to clay-rich assemblages are represented by muscovite, phengite, and illite, whereas chlorite, epidote, and carbonate minerals characterize the propylitic assemblage. In the geological map, K-feldspar marks potassic alteration; in the four-mineral index, this domain is expressed by comparatively low values.

Table 2. *Alteration zones and diagnostic mineral assemblages.*

Attribute	Potassic-silicic zone	Phyllic zone	Propylitic zone
Diagnostic minerals	K-feldspar and muscovite	Muscovite and illite	Chlorite and carbonate minerals

4.2. Geological Reference Zonation

Published geological mapping depicts alteration around the mineralized porphyry as a broadly concentric system [15, 25]. Outward from the center, the mapped domains comprise potassic-silicic, phyllic, propylitic, illite-hydromuscovite, limonite, and hornfels zones. K-feldspar, muscovite, chlorite, epidote, and carbonate minerals provide the principal mineralogical markers. Figure 4 shows the simplified geological reference used to assess the spectral model.

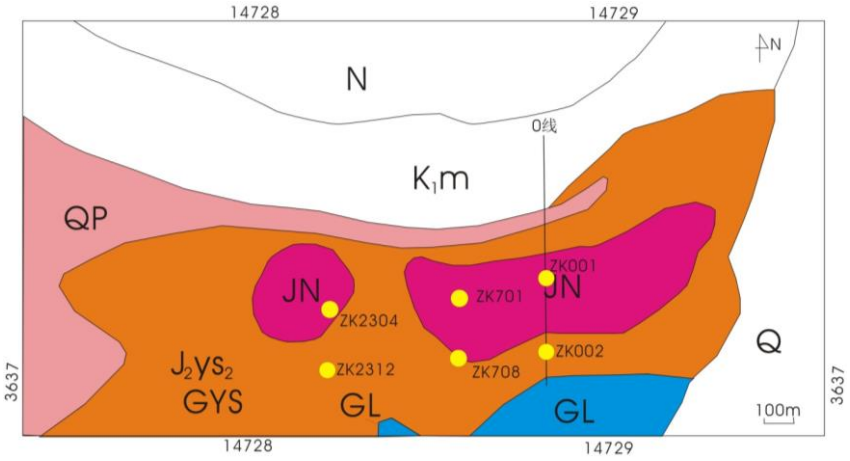

Figure 4. *Geological reference map of horizontal alteration zonation at Duobuza.*

QP, propylitic zone; JN, superimposed potassic and clay alteration; GYS, silicification-illite-hydromuscovite zone; GL, silicification-chloritization zone; K1m, Lower Cretaceous Meiriqie Formation; Q, Quaternary.

4.3. Vertical Alteration Zonation

Index values calculated from the drill-core spectra define three main vertical domains. The lowest class is assigned to potassic-silicic alteration, the intermediate class to phyllic alteration, and the highest class to the chlorite- and carbonate-rich propylitic assemblage. These classified measurements form the basis of the three-dimensional distribution in Figure 5.

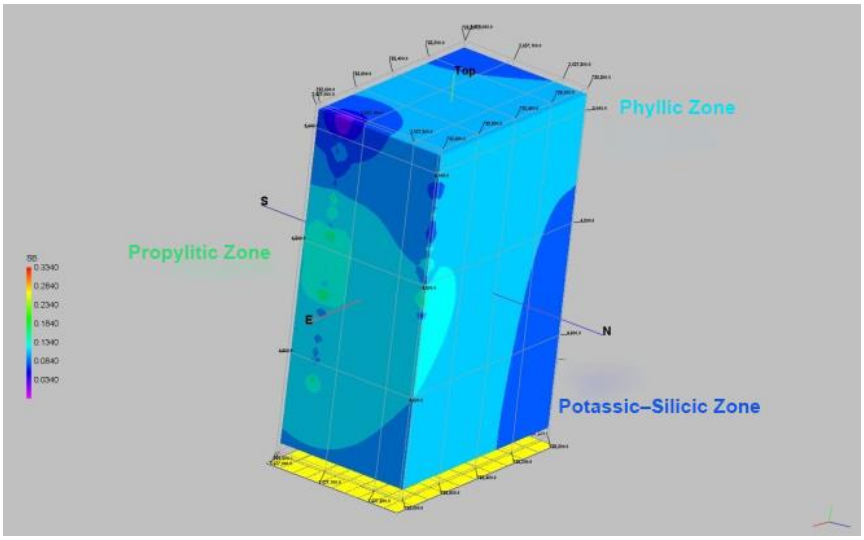

Labels denote the propylitic, phyllic and potassic-silicic alteration zones.

Figure 5. *Three-dimensional alteration-zonation model of the Duobuza deposit.*

4.4. Horizontal Alteration Zonation

Evaluation of Equation (1) for the 15 surface samples produced a semiquantitative map of horizontal zonation. Potassic-silicic alteration is concentrated in the north and northeast, where it broadly overlaps the intrusive rocks and mapped potassic alteration. Phyllic alteration occurs around these potassic centers, and a wider propylitic domain lies farther outward. The illite-hydromuscovite zone extends through the central and southern parts of the map. This approximately concentric arrangement agrees with geological mapping [25] and with the surface-based alteration pattern previously reported for Duolong [15].

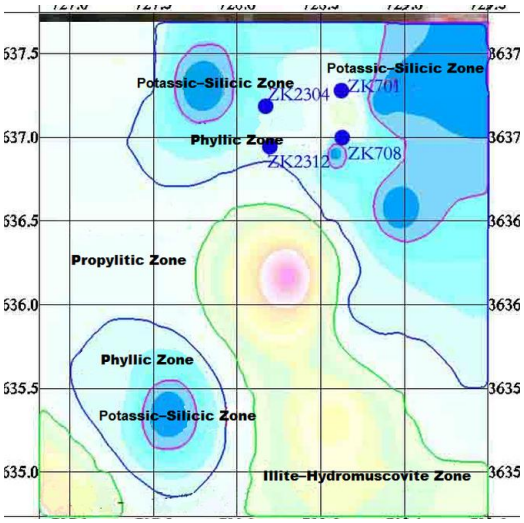

Figure 6. *Horizontal alteration zonation derived from surface reflectance spectra.*

Labels denote potassic-silicic, phyllic, propylitic and illite-hydromuscovite zones.

4.5. Relationship Between Alteration Index and Cu

The index and Cu records exhibit an inverse spatial association. Areas assigned low index values in the potassic-silicic domain contain comparatively high Cu concentrations, whereas the high-index propylitic domain is associated with lower Cu concentrations. Cu grade therefore decreases outward from the potassic-silicic center toward the propylitic margin in the available profiles. Because sample-level statistical tests and uncertainty estimates were unavailable, this observation is treated as spatial correspondence and not as a calibrated predictive relationship.

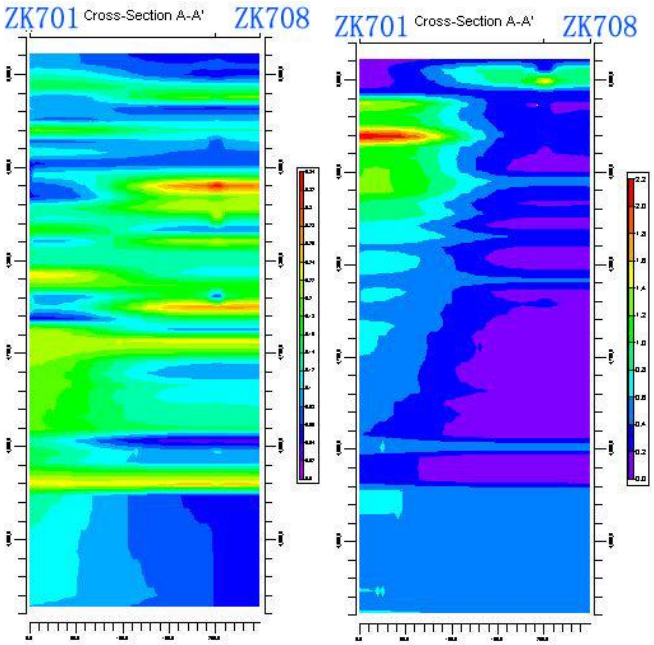

Figure 7. *Cross-sectional comparison of alteration index and Cu concentration between ZK701 and ZK708.*

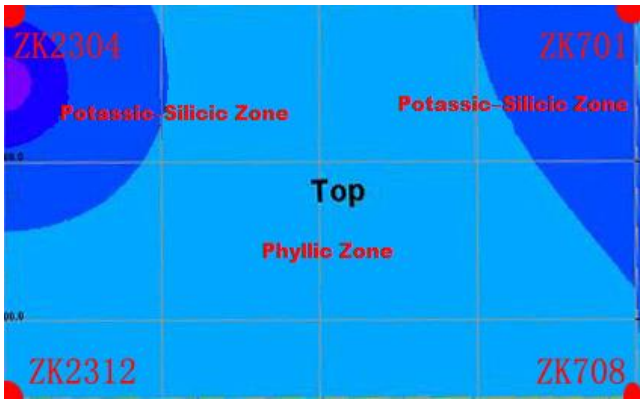

Labels identify the potassic-silicic and phyllic alteration zones around ZK2304, ZK2312, ZK701 and ZK708.

Figure 8. *Comparison between the modelled horizontal alteration pattern and geological mapping.*

5. Discussion

5.1. Interpretation of the Alteration Zonation

The drill-core and surface spectra recover the main alteration architecture documented at Duobuza: a potassic-silicic domain near the mineralized center, an intervening phyllic domain, and an outer propylitic assemblage rich in chlorite and carbonate. The same first-order organization is present in published surface-based alteration mapping [15, 25] and is compatible with fluid-inclusion evidence for a high-temperature magmatic-hydrothermal system [20, 22, 23]. The index is an empirical summary of the relative behavior of four spectrally identified minerals; it should not be interpreted as a thermometer or as a direct measure of absolute alteration intensity.

5.2. Comparison and Exploration Significance

Earlier multispectral and hyperspectral investigations of Duolong focused primarily on alteration visible at the ground surface [12-18]. Drill-core spectroscopy adds the missing depth dimension and therefore enables a three-dimensional interpretation. At Duobuza, the spatial coincidence of low index values, potassic-silicic alteration, and comparatively high Cu concentrations may help locate the mineralized center when the vertical and horizontal models are considered together. The index alone, however, cannot be used to predict Cu grade quantitatively.

5.3. Limitations and Further Work

The vertical model is based on four Duobuza drill holes, and the horizontal model is based on 15 irregularly spaced surface samples. The drill-core scanning density and surface sampling intervals require further improvement. In addition, minerals associated with surface weathering, including gypsum, halloysite, and montmorillonite, may differ from the hypogene alteration assemblage recorded in drill core. Denser spectral measurements and closer integration with geological, geochemical, geophysical, and satellite remote-sensing data are therefore needed to refine the model.

6. Conclusions

The Duobuza spectra contain an alteration assemblage of anhydrite, gypsum, muscovite, phengite, chlorite, epidote, calcite, halloysite, montmorillonite, and illite. Combining the relative abundances of illite, chlorite, muscovite, and calcite in an empirical index allowed drill-core and surface measurements to be classified within a common framework.

This classification resolves potassic-silicic, phyllic, and propylitic domains. Integrating their vertical and horizontal distributions yields a three-dimensional zonation that broadly agrees with the available geological map.

Within the available profiles, low index values in the potassic-silicic domain coincide with higher Cu concentrations, while the high-index propylitic domain contains lower Cu concentrations. The zonation is therefore useful as a qualitative mineralization indicator, although the empirical index has not been calibrated to predict Cu grade.

The joint use of surface and drill-core spectra carries alteration mapping from exposed rocks into the subsurface. This semiquantitative three-dimensional framework can be refined by incorporating denser spectroscopy together with geological, geochemical, geophysical, and satellite remote-sensing observations.

Abbreviations

AI	Alteration Index
ASTER	Advanced Spaceborne Thermal Emission and Reflection Radiometer
Cu	Copper
OLI	Operational Land Imager
SWIR	Short-Wave Infrared
VNIR	Visible and Near-Infrared

Author Contributions

Zhengxuan Li: Investigation, Data curation, Formal analysis, Visualization, Writing – original draft

Fojun Yao: Conceptualization, Methodology, Supervision, Project administration, Funding acquisition, Writing – review & editing

Funding

This work is supported by the Major Special Project of Xinjiang Uygur Autonomous Region (Grant No. 2022A03009-3) and the China Geological Survey Project (Grant No. DD202602109203).

Conflicts of Interest

The authors declare no conflicts of interest

References

[1] Hunt, G. R. Spectral signatures of particulate minerals in the visible and near infrared. Geophysics, 1977, 42(3): 501-513. https://doi.org/10.1190/1.1440721

[2] Hunt, G. R. Near-infrared (1.3-2.4 micrometers) spectra of alteration minerals: Potential for use in remote sensing. Geophysics, 1979, 44(12): 1974-1986. https://doi.org/10.1190/1.1440951

[3] Clark, R. N., Roush, T. L. Reflectance spectroscopy: Quantitative analysis techniques for remote sensing applications. Journal of Geophysical Research, 1984, 89(B7): 6329-6340. https://doi.org/10.1029/JB089iB07p06329

[4] Thompson, A. J. B., Hauff, P. L., Robitaille, A. J. Alteration mapping in exploration: Application of short-wave infrared spectroscopy. SEG Newsletter, 1999, 39: 1, 16-27. https://doi.org/10.5382/SEGnews.1999-39.fea

[5] Tong, Q. X., et al. Spectra and Analysis of Typical Earth Objects of China. Beijing: Science Press, 1990. ISBN 978-7-03-002030-7. (in Chinese).

[6] Nie, F. J., Jiang, S. H., Zhao, S. M. Application of short-infrared spectroscopy to mineral-resource assessment. Geology in China, 2000, (4): 38-42. (in Chinese).

[7] Zhang, G., Lian, C. Y., Yuan, C. H. Application of PIMA to mineral identification at the Pulang porphyry copper deposit, Yunnan. Earth Science Frontiers, 2004, 11(4): 460. (in Chinese).

[8] Zhang, G., Lian, C. Y., Wang, R. S. Application of a portable infrared mineral analyzer to mineral mapping in the Qulong copper district, Mozhugongka County, Tibet. Geological Bulletin of China, 2005, 24(5): 480-484. (in Chinese).

[9] Lian, C. Y., Zhang, G., Yuan, C. H. Application of SWIR reflectance spectroscopy to Pulang porphyry copper ore district, Yunnan Province. Mineral Deposits, 2005, 24(6): 621-637. (in Chinese with English abstract).

[10] Wang, S. D., Liu, S. H., Li, X., Tang, Y. M., Yu, K. Methodological considerations for field spectral measurements. Remote Sensing Information, 2006, (1): 29-33. https://doi.org/10.3969/j.issn.1000-3177.2006.01.008 (in Chinese).

[11] Yao, F. J. The Study of Remote Sensing Alteration Zoning Models of Typical Porphyry Copper Deposits in China. Beijing: China University of Geosciences (Beijing), 2012. (in Chinese).

[12] Hu, Z. H., Tang, J. X., Zhang, T. B., Wu, H., Xu, Z. Z., Bie, X. J. Characteristics of remote sensing alteration anomalies from ASTER in the Duobuza porphyry copper deposit. Remote Sensing for Land and Resources, 2012, 24(1): 150-154. https://doi.org/10.6046/gtzyyg.2012.01.26 (in Chinese with English abstract).

[13] Dai, J. J., Wang, R. J., Qu, X. M., Xin, H. B. Application of TerraSpec spectrometer to the study of alteration information in the Duobuza porphyry copper deposit of Tibet. Remote Sensing for Land and Resources, 2013, 25(1): 105-110. https://doi.org/10.6046/gtzyyg.2013.01.19 (in Chinese with English abstract).

[14] Zhang, T. B., Yi, G. H., Li, H. M., Wang, Z. Y., Tang, J. X., Zhong, K. H., Li, Y. B., Wang, Q., Bie, X. J. Integrating data of ASTER and Landsat-8 OLI (AO) for hydrothermal alteration mineral mapping in Duolong porphyry Cu-Au deposit, Tibetan Plateau, China. Remote Sensing, 2016, 8(11): 890. https://doi.org/10.3390/rs8110890

[15] Yao, F., Xu, X., Yang, J., Geng, X. A remote-sensing-based alteration zonation model of the Duolong porphyry copper ore district, Tibet. Remote Sensing, 2021, 13(24): 5073. https://doi.org/10.3390/rs13245073

[16] Dong, X., Gan, F., Li, N., Zhang, S., Li, T. Mineral mapping in the Duolong porphyry and epithermal ore district, Tibet, using Gaofen-5 satellite hyperspectral remote-sensing data. Ore Geology Reviews, 2022, 151: 105222. https://doi.org/10.1016/j.oregeorev.2022.105222

[17] Fu, Y., Cheng, Q., Jing, L., Ye, B., Fu, H. Mineral prospectivity mapping of porphyry copper deposits based on remote-sensing imagery and geochemical data in the Duolong ore district, Tibet. Remote Sensing, 2023, 15(2): 439. https://doi.org/10.3390/rs15020439

[18] Chen, Q., Cai, D., Xia, J., Zeng, M., Yang, H., Zhang, R., He, Y., Zhang, X., Chen, Y., Xu, X., Zhao, Z. Remote-sensing identification of hydrothermal alteration minerals in the Duobuza porphyry copper mining area in Tibet using WorldView-3 and GF-5 data: The impact of spatial and spectral resolution. Ore Geology Reviews, 2025, 180: 106573. https://doi.org/10.1016/j.oregeorev.2025.106573

[19] Wang, P. J., Mattern, F., Schneider, W., Liu, W. S., Tian, W. Q., Li, C. The Cretaceous of the eastern Bangong-Nujiang suture zone (Tibet): Tectono-sedimentation. Global Geology, 2003, 22(2): 105-110. (in Chinese with English abstract).

[20] Li, G. M., Li, J. X., Qin, K. Z., Zhang, T. P., Xiao, B. High temperature, salinity and strong oxidation ore-forming fluid at Duobuza gold-rich porphyry copper deposit in the Bangonghu tectonic belt, Tibet: Evidence from fluid inclusions. Acta Petrologica Sinica, 2007, 23(5): 935-952. (in Chinese with English abstract).

[21] Li, J. X., Li, G. M., Qin, K. Z., Xiao, B. Geochemistry of porphyries and volcanic rocks and ore-forming geochronology of Duobuza gold-rich porphyry copper deposit in Bangonghu belt, Tibet: Constraints on metallogenic tectonic settings. Acta Petrologica Sinica, 2008, 24(3): 531-543. (in Chinese with English abstract).

[22] She, H. Q., Li, J. W., Feng, C. Y., Ma, D. F., Pan, G. T., Li, G. M. The high-temperature and hypersaline fluid inclusions and its implications to the metallogenesis in Duobuza porphyry copper deposit, Tibet. Acta Geologica Sinica, 2006, 80(9): 1434-1447. (in Chinese with English abstract).

[23] Li, J. X., Li, G. M., Qin, K. Z., Xiao, B. High temperature primary magmatic fluid directly exsolved from magma at Duobuza gold-rich porphyry copper deposit, northern Tibet. Geofluids, 2011, 11(2): 134-143. https://doi.org/10.1111/j.1468-8123.2011.00325.x

[24] Li, J. X., Qin, K. Z., Li, G. M., Xiao, B., Zhao, J. X., Chen, L. Magmatic-hydrothermal evolution of the Cretaceous Duolong gold-rich porphyry copper deposit in the Bangongco metallogenic belt, Tibet: Evidence from U-Pb and 40Ar/39Ar geochronology. Journal of Asian Earth Sciences, 2011, 41(6): 525-536. https://doi.org/10.1016/j.jseaes.2011.03.008

[25] Li, G. M., Li, J. X., Qin, K. Z., Duo, J., Zhang, T. P., Xiao, B., Zhao, J. X. Geology and hydrothermal alteration of the Duobuza gold-rich porphyry copper district in the Bangongco metallogenetic belt, northwestern Tibet. Resource Geology, 2012, 62(1): 99-118. https://doi.org/10.1111/j.1751-3928.2011.00182.x